# On the importance of surface forcing in conceptual models of the deep ocean

Andrew L. Stewart*

*Environmental Sciences and Engineering, California Institute of Technology, Pasadena, California*

Raffaele Ferrari

*Department of Earth, Atmospheric, and Planetary Sciences, Massachusetts Institute of Technology, Cambridge, Massachusetts*

Andrew F. Thompson

*Environmental Sciences and Engineering, California Institute of Technology, Pasadena, California*

ABSTRACT

In the major ocean basins, diapycnal mixing upwells dense Antarctic Bottom Water, which returns southward and closes the deepest cell of the meridional overturning circulation (MOC). This cell ventilates the deep ocean and regulates the partitioning of $CO_2$ between the atmosphere and the ocean. Our conceptual understanding of the deep stratification and MOC has evolved from classic "abyssal recipes" arguments to a more recent appreciation of along-isopycnal upwelling in the Southern Ocean, consistent with a weakly-mixed ocean interior. Both the deep stratification and the deep MOC are here shown to be sensitive to the form of the surface buoyancy forcing in a two-dimensional model that includes a circumpolar channel and northern basin. For a fixed surface buoyancy condition, the deep stratification is essentially prescribed, whereas for a fixed surface buoyancy flux, the deep stratification varies by orders of magnitude over the range of $\kappa$ observed in the ocean. These cases also produce different scalings for the deep MOC with $\kappa$, in both weak and strong $\kappa$ regimes. In addition, these scalings are shown to be sensitive not only to the type of surface boundary condition, but also to the latitudinal structure of the surface fluxes. This latter point is crucial as buoyancy budgets and dynamical features of the circulation are poorly constrained along the Antarctic margins. This study emphasizes the need for caution in the interpretation of simple conceptual models that, while useful, may not include all mechanisms that contribute to the MOC's strength and structure.

## 1. Introduction

Conceptual models have clarified scientific understanding of the ocean's deep stratification and meridional overturning circulation (MOC), while making predictions that may be tested via observations and numerical modeling. Our conceptual understanding has evolved, with two end points being the uniform vertical advective-diffusive balance assumed by Munk (1966) and the theory posited by Nikurashin and Vallis (2011, hereafter NV11), sketched in Figure 1. This more recent view recognizes that the diapycnal diffusivity is an order of magnitude smaller than Munk's (1966) estimate (e.g. Ledwell et al. 1993), and so transport is typically directed along isopycnals in the ocean interior (Lumpkin and Speer 2007). The purpose of this note is to highlight that, while the NV11 conceptual model illustrates the importance of the Southern Ocean in the setting the global stratification and MOC, it may change dramatically with the with improved representation of the dynamics in this region, especially at the Antarctic margins. As an example, modification of the surface boundary condition over the Southern Ocean dramatically alters the sensitivities of the deep stratification and MOC to diapycnal mixing.

The deep cell of the MOC is supplied by the outflow of Antarctic Bottom Water (AABW, Gordon 2009), upwells via the action of diapycnal mixing and returns to the surface via outcropping isopycnal surfaces in the Southern Ocean (Lumpkin and Speer 2007). This circulation is of interest because it may control the ocean-atmosphere $CO_2$ partitioning over millennial time scales (Skinner et al. 2010). This has motivated a series of investigations of the sensitivity of the deep MOC, for example to changes in surface forcing (Stewart and Thompson 2012; Meredith et al. 2012).

The role of conceptual models is to summarize in a clear and accessible way the mechanisms that control the deep stratification and MOC. Munk's (1966) landmark study assumed the deep circulation to consist of uniform upwelling

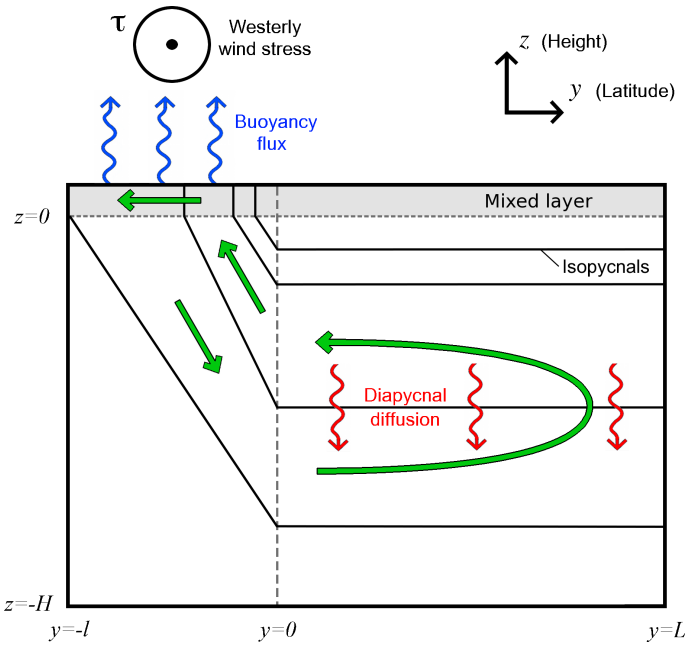


FIG. 1. A schematic of the residual-mean model of the deep overturning circulation. In the Southern Ocean channel ($y < 0$), the deep circulation is directed along isopycnals, and is constructed as a residual of a wind-driven mean circulation that tends to steepen isopycnals, and and opposing "eddy" circulation that relaxes isopycnals by releasing potential energy through baroclinic instability (Karsten and Marshall 2002). The circulation is closed by buoyancy loss to the atmosphere, which supports a southward diabatic transport in the surface mixed layer, and by downward diapycnal diffusion of buoyancy in the northern basin ($y > 0$), which supports upwelling across isopycnal surfaces.

supported by downward diffusive fluxes, and established that a vertical diffusivity of $\kappa \approx 1 \times 10^{-4}\,\mathrm{m^2\,s^{-1}}$ was required to balance the export of AABW. This model dominated thinking for decades until direct measurements of mixing rates in the upper ocean established that the diffusivity is closer to $\kappa \approx 1 \times 10^{-5}\,\mathrm{m^2\,s^{-1}}$ (Ledwell et al. 1993). The implication that transport in the ocean interior is largely along isopycnals emphasizes the role of the Southern Ocean in closing water mass pathways, and is reflected in models like that of Gnanadesikan (1999), later extended to include the deep cell by Shakespeare and Hogg (2012). Ito and Marshall (2008) proposed a residual-mean model in which lateral mixing by mesoscale eddies and enhanced diapycnal mixing at depth constrain water mass transformation in the deep ocean, and thus the strength of the deep MOC.

The most recent dynamically-consistent model of the deep cell is that of NV11, which agrees qualitatively with observations of the deep MOC (Lumpkin and Speer 2007). Their scalings for the sensitivity of the deep stratification and MOC to diapycnal mixing are corroborated by coarse-resolution simulations with a Gent and McWilliams (1990) parameterization, and agree qualitatively with the eddy-resolving simulations conducted by Munday et al. (2013). Here we identify the Southern Ocean surface buoyancy condition as an unexplored, but critical, component of this model that has received little attention and is poorly understood.

We demonstrate that a straightforward but plausible change in the surface boundary condition in a NV11-like configuration qualitatively changes the properties of the model. NV11 apply a fixed buoyancy profile at the ocean surface, which is a suitable approximation for the strong restoring to atmospheric temperature acting along the Antarctic Circumpolar Current latitudes (Haney 1971). However, this boundary condition is not appropriate for the coastal regions of Antarctica in which AABW is formed. For example, brine rejection in near-shore polynyas may be more closely approximated as a fixed surface buoyancy flux (Chapman 1999; Wilchinsky and Feltham 2008). Here we contrast the sensitivity of the model's deep stratification and MOC to the diapycnal diffusivity $\kappa$ in the limiting cases of a prescribed surface buoyancy versus a prescribed surface flux.

## 2. Scalings for deep stratification and overturning

### a. *Residual-mean model*

We employ the conceptual model of NV11, illustrated in Figure 1. For simplicity we restrict our attention to the deepest cell of the MOC, which is permitted to occupy the entire water column. We could restrict the deep cell to below 2–3 km depth, as in the real ocean, but our results would not change qualitatively.

Following NV11, the stratification and overturning in the Southern Ocean "channel" portion $-l < y < 0$ of our model domain are governed by

$$J(\psi, b) = \kappa b_{zz}, \tag{1a}$$

$$\psi = -\frac{\tau}{\rho_0 f} + Ks, \tag{1b}$$

$$\psi = -\kappa L \frac{b_{zz}}{b_z} \quad \text{on} \quad y = 0. \tag{1c}$$

Equation (1a) balances advective transport of the time- and zonal-mean buoyancy $b$ by a streamfunction $\psi$ with vertical diffusion $\kappa$ across buoyancy surfaces. The advecting streamfunction is a small residual (1b) of a wind-driven mean overturning, proportional to the surface wind stress $\tau$, and an opposing eddy overturning proportional to the isopycnal slope $s = -b_y/b_z$ (Marshall and Radko 2003; Plumb and Ferrari 2005). We denote the reference density as $\rho_0$, the Coriolis parameter as $f$, and the isopycnal

and diapycnal diffusivities as $K$ and $\kappa$ respectively. We obtain the boundary condition (1c) at $y = 0$ by assuming zero isopycnal slope in the northern basin ($b_y \equiv 0$), and integrating (1a) from $y = 0$ to $y = L$. To simplify the presentation we have taken $\tau$, $K$, $\kappa$, and $f$ to be constants; in the real ocean these quantities vary by orders of magnitude.

In the limit of a small residual overturning streamfunction the two terms on the right-hand side of (1b) balance at leading order and prescribe a uniform isopycnal slope in the channel,

$$s = \frac{\tau}{\rho_0 f K} = \text{constant}. \tag{2}$$

This approximation holds under the assumption that the diffusively-driven residual overturning is much weaker than the wind-driven mean overturning,

$$\varepsilon = \frac{\kappa K L \rho_0^2 f^2}{l \tau^2} \ll 1. \tag{3}$$

Here we scaled $\psi$ using the right-hand side of (1c), using $h \sim l \cdots$ as a vertical scale for the stratification.

We also assume that the northern basin is much wider than the channel, as is the case in the real ocean,

$$\delta = \frac{l}{L} \ll 1. \tag{4}$$

Under this assumption we may neglect the right-hand side of (1a),

$$J(\psi, b) = 0 \implies \psi = \psi(b), \tag{5}$$

which states that the residual streamfunction is constant along isopycnals in the channel. It follows from (5) and (2) that the buoyancy and streamfunction can be mapped between $z = 0$ and $y = 0$ via

$$b(0, z) = b(-z/s, 0), \qquad \psi(0, z) = \psi(-z/s, 0). \tag{6}$$

*b. Fixed surface buoyancy*

NV11 studied the case of a prescribed surface buoyancy profile,

$$b = b_s(y) \quad \text{on} \quad z = 0. \tag{7}$$

They argue that this is a suitable approximation in regions where temperature dominates the buoyancy variations and restoring to the atmosphere is fast.

From (6) it follows that the buoyancy in the northern basin is prescribed by the surface buoyancy profile,

$$b(0, z) = b_s(-z/s). \tag{8}$$

The stratification in the northern basin is therefore prescribed by the surface buoyancy profile,

$$N^2(z) = -\frac{1}{s} \left. \frac{\mathrm{d}b_s}{\mathrm{d}y} \right|_{y=-z/s}, \tag{9}$$

so it is independent of the diapycnal diffusivity $\kappa$.

TABLE 1. List of parameters used in our analytical scaling and numerical solutions.

| Symbol | Value | Description |
|---|---|---|
| $L$ | $10000\,\mathrm{km}$ | Northern basin width |
| $l$ | $2000\,\mathrm{km}$ | Channel width |
| $H$ | $5000\,\mathrm{m}$ | Ocean depth |
| $\rho_0$ | $1000\,\mathrm{kg\,m^{-3}}$ | Reference density |
| $C_p$ | $4000\,\mathrm{J\,K^{-1}\,kg^{-1}}$ | Specific heat capacity |
| $\alpha$ | $2 \times 10^{-4} K^{-1}$ | Thermal expansion coefficient |
| $g$ | $9.81\,\mathrm{m^2\,s^{-1}}$ | Gravitational constant |
| $f$ | $-1 \times 10^{-4}\,\mathrm{s^{-1}}$ | Coriolis parameter |
| $\tau$ | $0.1\,\mathrm{N\,m^{-2}}$ | Surface wind stress |
| $Q_0$ | $10\,\mathrm{W\,m^{-2}}$ | Surface energy flux |
| $K$ | $1000\,\mathrm{m^2\,s^{-1}}$ | Isopycnal diffusivity |
| $M^2$ | $5 \times 10^{-9}\,\mathrm{s^{-2}}$ | Minimum lateral stratification |
| $\gamma$ | $10^{-14}\,\mathrm{m^{-1}\,s^{-2}}$ | Lateral stratification gradient |

We may similarly combine (7) with the northern boundary condition (1c) to obtain an expression for the surface residual streamfunction,

$$\psi = \frac{\kappa L}{s} \frac{\mathrm{d}_{yy} b_s}{\mathrm{d}_y b_s} \quad \text{on} \quad z = 0. \tag{10}$$

At any fixed latitude $y$, the overturning $\psi$ scales linearly with $\kappa$. The latitude of the surface streamfunction maximum $\psi_{\max}$ is determined by $\partial_y \psi(y_{\max}, 0) = 0$, so $y_{\max}$ is independent of $\kappa$. Therefore the deep MOC strength should scale linearly with $\kappa$, in agreement with the findings of NV11. Intuitively this is because the surface buoyancy profile sets deep stratification, which in turn sets the structure of the overturning streamfunction by (1c).

*c. Fixed surface flux*

We now consider the case of a fixed surface buoyancy flux at the ocean surface. This is arguably a more appropriate boundary condition where salinity plays an important role in setting buoyancy variations, like under ice.

Following Marshall and Radko (2003) we assume zero stratification in the mixed layer ($b_z \equiv 0$) and integrate (1a) from the base of the mixed layer ($z = 0$) to the ocean surface,

$$\psi = \frac{B(y)}{b_y} \quad \text{on} \quad z = 0. \tag{11}$$

Here $B$ is the downward buoyancy flux into the ocean surface. We will restrict our attention to the case of surface buoyancy loss, $B \leq 0$. Using (6) along with (1c) we obtain

$$b_{yy} = \frac{s}{\kappa L} B \quad \text{on} \quad z = 0. \tag{12}$$

Integrating once with respect to $y$ yields the surface lateral

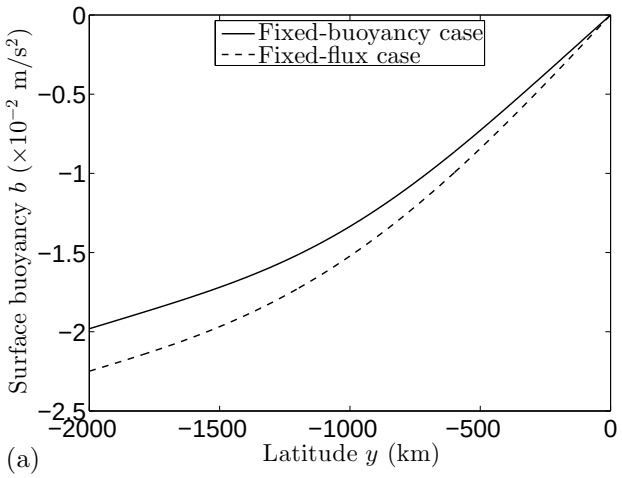


(a)

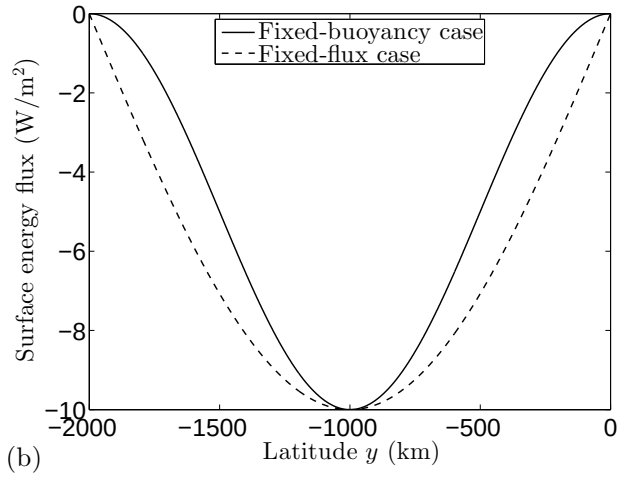


(b)

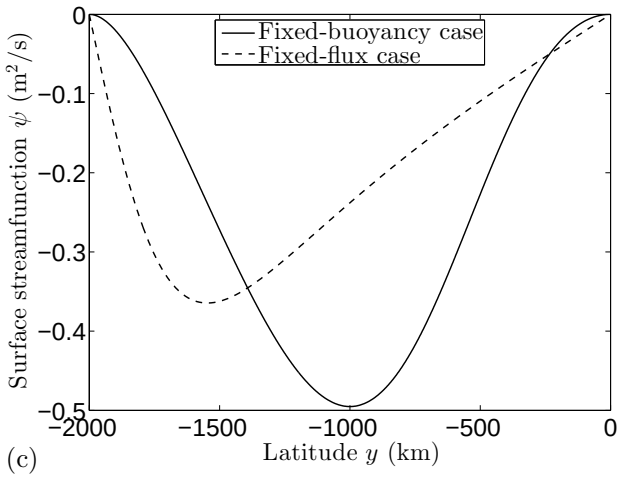


(c)

FIG. 2. Plots of surface properties in the Southern Ocean channel: (a) the buoyancy profile $b_s$, (b) the downward buoyancy flux, converted to an equivalent energy flux $Q = \rho_0 C_p B/\alpha g$, and (c) the streamfunction $\psi$, as derived in §2. In each case the diapycnal diffusivity is $\kappa = 5\times10^{-5}\,\mathrm{m^2\,s^{-1}}$.

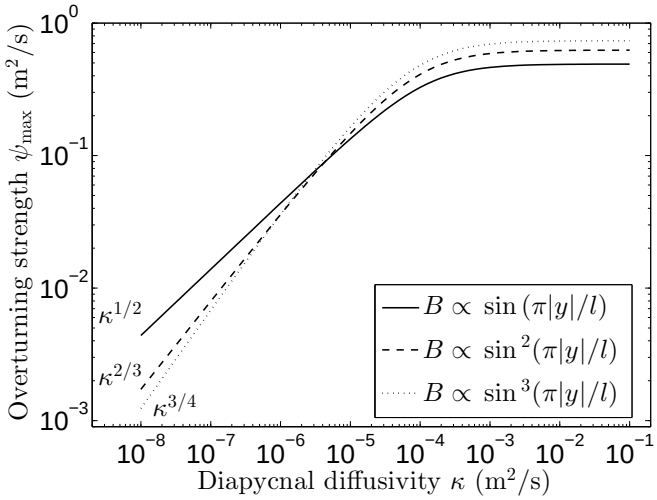


FIG. 3. Dependence of the maximum overturning $\psi_{\max} = \max_{y,z}|\psi|$ on the diapycnal diffusivity $\kappa$ for different surface buoyancy flux profiles $B(y)$. The total buoyancy loss at the ocean surface is the same for each profile. The parameters otherwise match those listed in Table 1.

stratification,

$$b_y|_{z=0} = M^2 + \frac{s}{\kappa L}\mathcal{B}(y), \qquad \mathcal{B}(y) = \int_{-l}^{y} B(y')\,\mathrm{d}y', \quad (13)$$

where $M^2 = b_y|_{y=-l,z=0}$ is the minimum lateral buoyancy gradient. Substituting (13) into (11) yields the surface streamfunction,

$$\psi = \frac{B(y)}{M^2 + \dfrac{s}{\kappa L}\mathcal{B}(y)} \quad \text{on} \quad z = 0. \quad (14)$$

In Figure 2 we contrast the solutions produced from a fixed surface buoyancy profile

$$\frac{\mathrm{d}b_s}{\mathrm{d}y} = M^2 + \tfrac{1}{2}\gamma\left(1 + \frac{y}{l}\right) + \frac{\gamma l}{4\pi}\sin\left(\frac{2\pi y}{l}\right), \quad (15)$$

versus a fixed surface buoyancy flux,

$$B(y) = -B_0 \sin\left(\frac{-\pi y}{l}\right). \quad (16)$$

We could modify $b_s(y)$ and $B(y)$ such that fixed-buoyancy and fixed-flux cases in Figure 2(a–b) agree even more closely. We have chosen (15) and (16) because they are simple, produce overturning streamfunctions of similar strength that vanish at $y = -l$ and $y = 0$, and yield robust numerical result in §3. Our parameter choices are listed in Table 1.

As the buoyancy flux is always directed out of the ocean ($B \le 0$), it follows from (12) that the stratification maximum lies at $y = z = 0$. Substituting $y = 0$ into (13) and

dividing by $-s$ we obtain the maximum stratification,

$$N^2_{\max} = -\frac{M^2}{s} - \frac{\mathcal{B}(0)}{\kappa L}. \tag{17}$$

Intuitively, the net diffusive buoyancy flux convergence in the northern basin must balance the net buoyancy loss at the ocean surface.

As in the prescribed-buoyancy case, at any fixed latitude $y$ the streamfunction (14) scales linearly with diffusivity $\kappa$ when $\kappa$ is sufficiently small. However, the form of (14) implies that the latitude at which the streamfunction maximum lies itself depends on the diffusivity, $y_{\max} = y_{\max}(\kappa)$ (here the "maximum" of $\psi$ refers to its most negative value). For example, a maximum of $\psi$ always exists close to $y = -l$: for a surface buoyancy flux that satisfies $B(y) \to C(y+l)^p$ as $y \to -l$ for some constant $C$, the streamfunction (14) is maximized at

$$y_{\max} = -l + \left[\frac{M^2 p(p+1)\kappa L}{Cs}\right]^{1/(p+1)}, \tag{18}$$

so there exists an maximum of $\psi$ that approaches the southern boundary $y = -l$ as $\kappa \to 0$. Substituting (18) into (14), we find that the overturning scales as $\psi_{\max} \sim \kappa^{p/(p+1)}$ for small $\kappa$. In general $\psi$ may have local maxima at other latitudes, but it follows from (14) that any other maximum satisfies $\psi_{\max} \sim \kappa \ll \kappa^{p/(p+1)}$ as $\kappa \to 0$, so for sufficiently small $\kappa$ the extremum close to $y = -l$ is the global maximum. Thus the dependence of the deep MOC strength on diapycnal mixing depends not only upon whether the surface buoyancy fluxes are fixed, but also upon the latitudinal structure of the fluxes. We illustrate this point in Figure 3, which shows the sensitivity of the MOC to diapycnal mixing for different buoyancy flux profiles.

## 3. Numerical sensitivity to diapycnal mixing

### *a. Numerical configuration*

The scalings derived in §2 are only valid for small $\varepsilon \ll 1$, or equivalently for small $\kappa$. To obtain a more general picture of the dependence of the deep MOC on diapycnal mixing, we now solve the residual-mean equations (1a)–(1c) and (7), (11) numerically. We obtain a steady solution of (1a) by integrating its time-dependent equivalent to steady state,

$$b_t + J(\psi, b) = \kappa b_{zz}. \tag{19}$$

Our numerical approach follows that of Stewart and Thompson (2013).

We apply boundary conditions of no-normal-flow ($\psi = 0$) at $y = -l$ and $z = -H$. An intuitive additional boundary condition at the ocean bed is that there should be no normal buoyancy flux, *i.e.* $b_z = 0$ at $z = -H$. However, by integrating (1c) vertically from $z = -H$ it may be shown that if the stratification vanishes at the bottom boundary, $b_z|_{z=-H} = 0$, then it must also vanish throughout the water column, $b_z \equiv 0$. Requiring no buoyancy flux through the bottom boundary is therefore incompatible with our assumption of flat isopycnals in the northern basin. Rather than complicate the NV11 model with a more sophisticated bottom boundary condition, we simply prescribe the stratification at $z = -H$, under the assumption that the ocean is bounded below by a boundary layer, or simply by more ocean,

$$b_z|_{z=-H} = N^2_{\text{bot}}. \tag{20}$$

For the case of fixed surface fluxes (11), we may simply choose $N^2_{\text{bot}} = 5 \times 10^{-6}\,\text{s}^{-1}$, which corresponds to $M^2 = 5 \times 10^{-9}\,\text{s}^{-2}$ using the parameters listed in Table 1. For the case of fixed surface buoyancy, we prescribe $N^2_{\text{bot}}$ to balance the steady-state buoyancy budget,

$$\int_{-l}^{L} [\psi_y b]_{z=0}\,\mathrm{d}y = \int_{-l}^{L} \left\{ \kappa b_z|_{z=0} - \kappa b_z|_{z=-H} \right\} \mathrm{d}y. \tag{21}$$

We approximate the surface terms in (21) using a uniform slope (2) and the analytical streamfunction (10), using continuity of $b_z$ at $y = 0$ to determine the surface stratification in the northern basin $0 < y < L$,

$$N^2_{\text{bot}} = \frac{L}{|s|(L+l)} \left.\frac{\mathrm{d}b_s}{\mathrm{d}y}\right|_{y=-l} + \frac{1}{|s|(L+l)} [b_s]^0_{-l}. \tag{22}$$

Note that the buoyancy profile (15) ensures that the streamfunction $\psi$ vanishes at $y = 0$, so there is no advective buoyancy exchange with the mixed layer in the northern basin.

Rather than impose (7) or (11) directly on $z = 0$, we have found that the stability and accuracy of the solution are improved by enforcing these conditions over a layer of finite depth $H_s = 100\,\text{m}$ close to the surface. For the fixed-flux case (11) we impose a downward buoyancy flux $B$ that decreases linearly in magnitude from $z = 0$ to $z = -H_s$. For the fixed-buoyancy case (7) we replace the fixed buoyancy flux $B$ with a relaxative flux $W_s(b - b_s)$. The surface piston velocity $W_s = 5 \times 10^{-5}\,\text{m}\,\text{s}^{-1}$ restores the surface buoyancy with a timescale of around 3 weeks.

### *b. Sensitivity to diapycnal mixing*

In Figure 4 we plot the numerically-computed stratification and overturning in the fixed-buoyancy and fixed-flux cases, for $\kappa$ ranging over two orders of magnitude. Over this range the overturning at $y = 0$ varies by $0.68\,\text{m}^2\,\text{s}^{-1}$ in the fixed-buoyancy case, and only by $0.26\,\text{m}^2\,\text{s}^{-1}$ in the fixed-flux case. This is consistent with our scalings in §2, which suggest that the overturning should scale linearly with $\kappa$ in the fixed-buoyancy case, and as $\kappa^{1/2}$ in the fixed-flux case (see Figure 3). In contrast the stratification exhibits almost no change in the fixed-buoyancy case, but varies by an order of magnitude in the fixed-flux case.

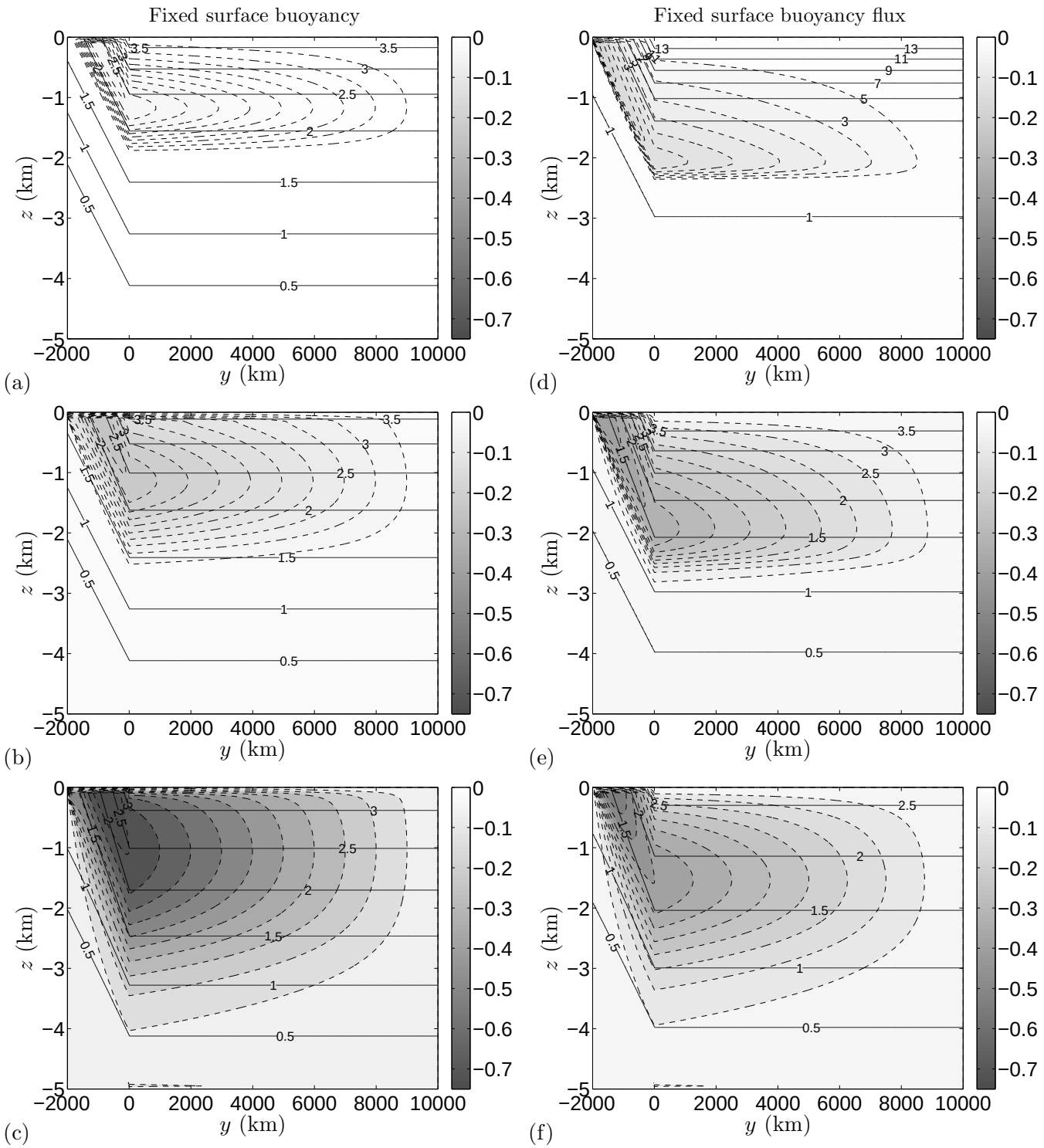


FIG. 4. Plots of the numerically-computed buoyancy $b$ in $10^{-2}\,\mathrm{m\,s^{-2}}$ (solid contours) and overturning streamfunction $\psi$ in $\mathrm{m^2\,s^{-1}}$ (dashed contours) for diapycnal diffusivities of (a,d) $\kappa = 5\times10^{-6}\,\mathrm{m^2\,s^{-1}}$, (b,e) $\kappa = 5\times10^{-5}\,\mathrm{m^2\,s^{-1}}$, and (c,f) $\kappa = 5\times10^{-4}\,\mathrm{m^2\,s^{-1}}$. The left-hand panels employ the fixed surface buoyancy profile (15), while the right-hand panels employ the fixed surface flux condition (16). All other parameters are listed in Table 1. Note the larger buoyancy contour intervals in panel (d). The dashed contour interval in each panel is one tenth of the maximum overturning strength.

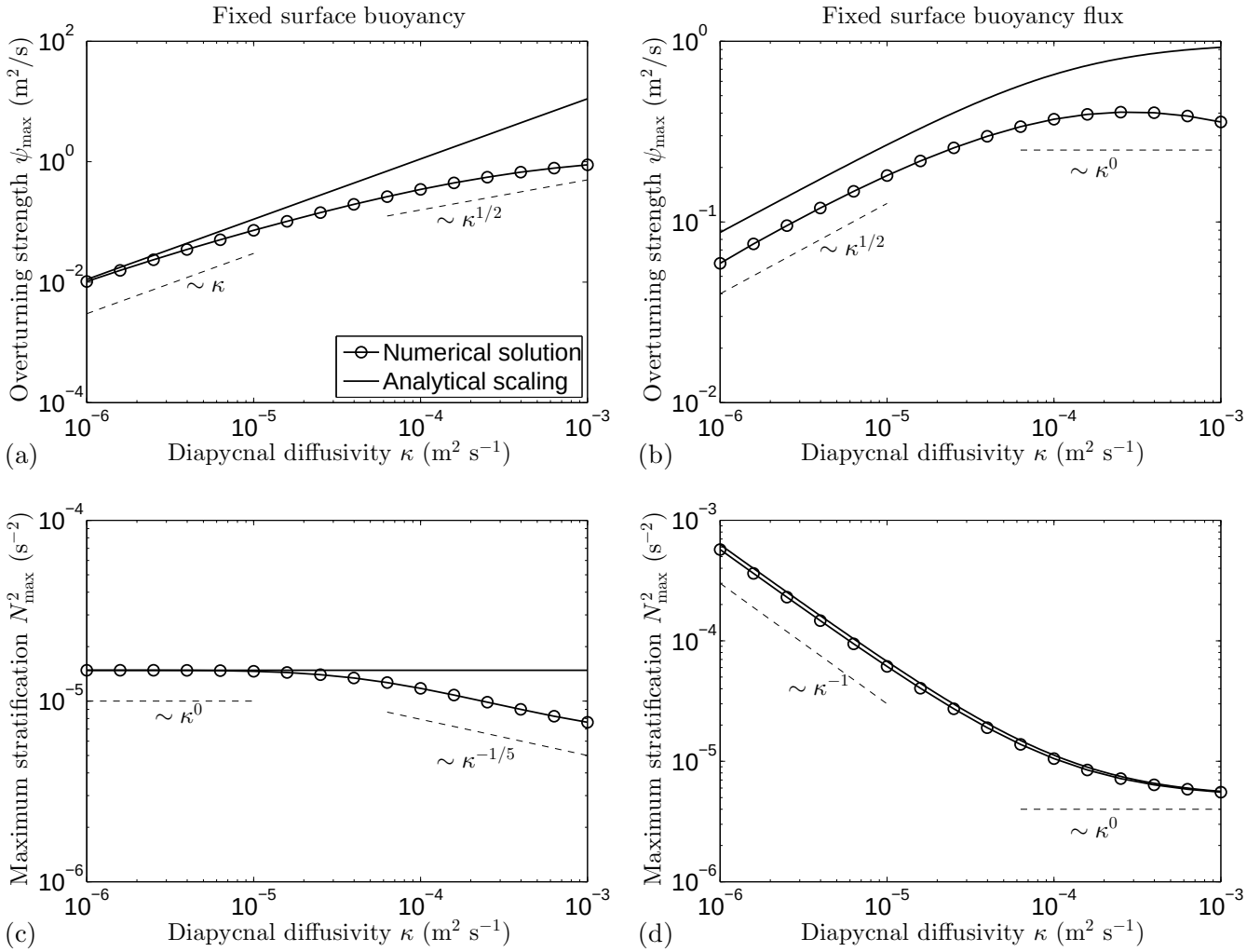


FIG. 5. Sensitivity of (a,b) the maximum overturning strength $\psi_{\max}$ and (c,d) the maximum stratification $N^2_{\max}$ in the northern basin to the rate of diapycnal mixing. The left-hand panels employ the fixed surface buoyancy profile (15), while the right-hand panels employ the fixed surface flux condition (16). For our numerical calculations we use the maximum overturning at the boundary between the channel and the northern basin, $\psi_{\max} = \max_{y=0} |\psi|$.

In Figure 5 we compare the numerically-calculated maximum overturning and stratification with the scalings derived in §2, for a range of $\kappa$ between $10^{-6}\,\mathrm{m^2\,s^{-1}}$ and $10^{-3}\,\mathrm{m^2\,s^{-1}}$. For $\kappa$ larger than this the overturning cell begins to interact with the bottom boundary. The scalings are quantitatively accurate as long as $\kappa$ is sufficiently small, as one would expect from the small-$\varepsilon$ approximation (3). The discrepancy between our scaling and the numerical results in Figure 5(b) is due to diffusive modification of the overturning streamfunction $\psi$ along isopycnals in the channel. Some discrepancy is present for all values of $\kappa$, no matter how small, because the maximum stratification scales as $N^2_{\max} \sim \kappa^{-1}$, and so the diffusive term on the right-hand side of (1a) is nonzero as $\kappa \to 0$.

In the fixed-buoyancy case the overturning appears to undergo transition to a large-$\kappa$ regime in which $\psi_{\max} \sim \kappa^{1/2}$, as in NV11. The stratification also undergoes a transition, scaling approximately as $N^2_{\max} \sim \kappa^{-1/5}$ for large $\kappa$. This transition is due to the fact that lateral transports in the channel are supported by eddy thickness fluxes, *i.e.* that the vertical isopycnal spacing must narrow in the direction of the residual transport. As $\kappa$ and $\psi$ increase, this effect begins to modify the stratification in the northern basin, which in turn impacts the overturning circulation. In the fixed-flux case both $\psi_{\max}$ and $N^2_{\max}$ agree qualitatively with our scalings from §2. For very large vertical mixing $\kappa$ the stratification becomes almost uniform and equal to $N^2_{\mathrm{bot}}$. This fixes the surface buoyancy gradient,

which in turn fixes the overturning circulation via (11).

## 4. Discussion

We have extended the conceptual model of NV11 to demonstrate that the sensitivities of the deep stratification $N^2_{\max}$ and MOC $\psi_{\max}$ to diapycnal mixing are themselves sensitive to the surface boundary condition. If the surface buoyancy is prescribed then we recover the results of NV11, in which $N^2_{\max}$ is effectively prescribed and $\psi_{\max}$ scales as $\kappa^1$ for small $\kappa$ and $\kappa^{1/2}$ for large $\kappa$. In contrast, if the surface fluxes are prescribed via (16) then $N^2_{\max}$ scales as $\kappa^{-1}$ for small $\kappa$, so varying $\kappa$ over the range observed in the ocean changes the stratification by orders of magnitude. The scaling for the overturning also changes, with $\psi_{\max}$ scaling as $\kappa^{1/2}$ for small $\kappa$ and as $\kappa^0$ for large $\kappa$. However, in the fixed-flux case the scaling of $\psi_{\max}$ with $\kappa$ also depends on the latitudinal structure of the flux, as shown in Figure 3. This complicates prediction of the deep MOC sensitivity to diapycnal mixing, as surface buoyancy fluxes are poorly constrained (Cerovecki et al. 2011).

For the purpose of illustration we have focused on one particular property of the NV11 model: its sensitivity to diapycnal mixing. A complete study would co-vary many of the model parameters, *e.g.* the wind stress $\tau$, eddy diffusivity $K$ and diapycnal diffusivity $\kappa$. NV11 argued that their model suggested that the deep ocean overturning is sensitive to diapycnal mixing rates, while the stratification is set by the surface boundary conditions in the Southern Ocean independently of diapycnal mixing. This result overturned the traditional view pioneered by Munk (1966), who argued that the ocean stratification is set by diapycnal mixing alone. We have shown that the result of NV11 depends on the choice of surface boundary condition. NV11 used a fixed buoyancy boundary condition, appropriate for waters that outcrop equatorward of the sea ice line and are strongly restored to atmospheric temperature. Switching to fixed flux boundary conditions more appropriate to describe the waters that outcrop around the Antarctic Continent, we find that both the stratification and overturning become sensitive to diapycnal mixing, but at rates depending on the specific latitudinal distribution of the fluxes. In reality the ocean surface is likely subject to a combination of these two boundary conditions. M. Nikurashin (personal communication) plans to extend our work in an upcoming paper and quantify the relative importance of these two forcings in the present ocean.

*Acknowledgments.*

A.L.S.'s and A.F.T.'s research was supported NSF award OCE-1235488. R.F. acknowledges support through NSF award OCE-1232962.

## REFERENCES

Cerovecki, I., L. D. Talley, and M. R. Mazloff, 2011: A comparison of Southern Ocean air-sea buoyancy flux from an ocean state estimate with five other products. *J. Climate*, **24 (24)**, 6283–6306.

Chapman, D. C., 1999: Dense Water Formation beneath a Time-Dependent Coastal Polynya. *J. Phys. Oceanogr.*, **29 (4)**, 807–820.

Gent, P. R. and J. C. McWilliams, 1990: Isopycnal mixing in ocean circulation models. *J. Phys. Oceanogr.*, **20 (1)**, 150–155.

Gnanadesikan, A., 1999: A simple predictive model for the structure of the oceanic pycnocline. *Science*, **283 (5410)**, 2077–2079.

Gordon, A. L., 2009: Bottom water formation. *Ocean Currents*, J. H. Steele, S. A. Thorpe, and K. K. Turekian, Eds., Associated Press, 263–269.

Haney, R. L., 1971: Surface thermal boundary condition for ocean circulation models. *J. Phys. Oceanogr.*, **1 (4)**, 241–248.

Ito, T. and J. Marshall, 2008: Control of lower-limb overturning circulation in the Southern Ocean by diapycnal mixing and mesoscale eddy transfer. *J. Phys. Oceanogr.*, **38 (12)**, 2832–2845.

Karsten, R. H. and J. Marshall, 2002: Constructing the residual circulation of the ACC from observations. *J. Phys. Oceanogr.*, **32 (12)**, 3315–3327.

Ledwell, J. R., A. J. Watson, and C. S. Law, 1993: Evidence for slow mixing across the pycnocline from an open-ocean tracer-release experiment. *Nature*, **364 (6439)**, 701–703.

Lumpkin, R. and K. Speer, 2007: Global ocean meridional overturning. *J. Phys. Oceanogr.*, **37 (10)**, 2550–2562.

Marshall, J. and T. Radko, 2003: Residual-mean solutions for the Antarctic Circumpolar Current and its associated overturning circulation. *J. Phys. Oceanogr.*, **33 (11)**, 2341–2354.

Meredith, M. P., A. C. Naveira Garabato, A. M. Hogg, and R. Farneti, 2012: Sensitivity of the overturning circulation in the Southern Ocean to decadal changes in wind forcing. *J. Climate*, **25 (1)**, 99–110.

Munday, D. R., H. L. Johnson, and D. P. Marshall, 2013: Eddy Saturation of Equilibrated Circumpolar Currents. *J. Phys. Oceanogr.*, **43**, 507–532.

Munk, W. H., 1966: Abyssal recipes. **13 (4)**, 707–730.

Nikurashin, M. and G. Vallis, 2011: A theory of deep stratification and overturning circulation in the ocean. *J. Phys. Oceanogr.*, **41 (3)**, 485–502.

Plumb, R. A. and R. Ferrari, 2005: Transformed Eulerian-mean theory. Part I: Nonquasigeostrophic theory for eddies on a zonal-mean flow. *J. Phys. Oceanogr.*, **35 (2)**, 165–174.

Shakespeare, C. J. and A. M. Hogg, 2012: An analytical model of the response of the meridional overturning circulation to changes in wind and buoyancy forcing. *J. Phys. Oceanogr.*, **42 (8)**, 1270–1287.

Skinner, L., S. Fallon, C. Waelbroeck, E. Michel, and S. Barker, 2010: Ventilation of the deep Southern Ocean and deglacial CO2 rise. *Science*, **328 (5982)**, 1147–1151.

Stewart, A. L. and A. F. Thompson, 2012: Sensitivity of the ocean's deep overturning circulation to easterly Antarctic winds. *Geophys. Res. Lett.*, **39 (18)**, L18 604.

Stewart, A. L. and A. F. Thompson, 2013: Connecting Antarctic Cross-Slope Exchange with Southern Ocean Overturning. *J. Phys. Oceanogr.*, **43**, 1453–1471.

Wilchinsky, A. V. and D. L. Feltham, 2008: Generation of a buoyancy-driven coastal current by an Antarctic polynya. *J. Phys. Oceanogr.*, **38 (5)**, 1011–1032.